Hsieh *et al. EJNMMI Research* 2022, **12**(1):43
https://doi.org/10.1186/s13550-022-00914-x

EJNMMI RESEARCH

ORIGINAL RESEARCH

Open Access

[^{18}F]ROStrace detects oxidative stress in vivo and predicts progression of Alzheimer's disease pathology in APP/PS1 mice

Chia-Ju Hsieh[1], Catherine Hou[1], Yi Zhu[2,3], Ji Youn Lee[1], Neha Kohli[2,3], Evan Gallagher[1,2,3], Kuiying Xu[1], Hsiaoju Lee[1], Shihong Li[1], Meagan J. McManus[2,3*] and Robert H. Mach[1*]

Abstract

Background Oxidative stress is implicated in the pathogenesis of the most common neurodegenerative diseases, such as Alzheimer's disease (AD). However, tracking oxidative stress in the brain has proven difficult and impeded its use as a biomarker. Herein, we investigate the utility of a novel positron emission tomography (PET) tracer, [^{18}F]ROStrace, as a biomarker of oxidative stress throughout the course of AD in the well-established APP/PS1 double-mutant mouse model. PET imaging studies were conducted in wild-type (WT) and APP/PS1 mice at 3 different time points, representing early (5 mo.), middle (10 mo.), and advanced (16 mo.) life ($n = 6$–12, per sex). Semi-quantitation SUVRs of the plateau phase (40–60 min post-injection; $SUVR_{40–60}$) of ten brain subregions were designated by the Mirrione atlas and analyzed by Pmod. Statistical parametric mapping (SPM) was used to distinguish brain regions with elevated ROS in APP/PS1 relative to WT in both sexes. The PET studies were validated by ex vivo autoradiography and immunofluorescence with the parent compound, dihydroethidium.

Results [^{18}F]ROStrace retention was increased in the APP/PS1 brain compared to age-matched controls by 10 mo. of age ($p < 0.0001$) and preceded the accumulation of oxidative damage in APP/PS1 neurons at 16 mo. ($p < 0.005$). [^{18}F]ROStrace retention and oxidative damages were higher and occurred earlier in female APP/PS1 mice as measured by PET ($p < 0.001$), autoradiography, and immunohistochemistry ($p < 0.05$). [^{18}F]ROStrace differences emerged midlife, temporally and spatially correlating with increased Aβ burden ($r^2 = 0.30$; $p = 0.0016$), which was also greatest in the female brain ($p < 0.001$).

Conclusions [^{18}F]ROStrace identifies increased oxidative stress and neuroinflammation in APP/PS1 female mice, concurrent with increased amyloid burden midlife. Differences in oxidative stress during this crucial time may partially explain the sexual dimorphism in AD. [^{18}F]ROStrace may provide a long-awaited tool to stratify at-risk patients who may benefit from antioxidant therapy prior to irreparable neurodegeneration.

Keywords Oxidative stress, Positron emission tomography, ROStrace, Alzheimer's disease, Neuroinflammation, Neurodegeneration

*Correspondence:
Meagan J. McManus
mcmanusm@email.chop.edu
Robert H. Mach
rmach@pennmedicine.upenn.edu
[1] Department of Radiology, Perelman School of Medicine, University of Pennsylvania, Philadelphia, PA 19104, USA
[2] Department of Anesthesiology and Critical Care Medicine, The Children's Hospital of Philadelphia, Philadelphia, PA 19104, USA
[3] Center for Mitochondrial and Epigenomic Medicine, The Children's Hospital of Philadelphia, Philadelphia, PA 19104, USA

Background

Alzheimer's disease (AD) is the most common neurodegenerative disease worldwide. Over the past 60 years, life expectancy in the USA has increased by almost a decade, tripling the number of people over the age of 65 to a record high of 50 million. One in ten of these individuals is diagnosed with AD, and two-thirds of

© The Author(s) 2022. **Open Access** This article is licensed under a Creative Commons Attribution 4.0 International License, which permits use, sharing, adaptation, distribution and reproduction in any medium or format, as long as you give appropriate credit to the original author(s) and the source, provide a link to the Creative Commons licence, and indicate if changes were made. The images or other third party material in this article are included in the article's Creative Commons licence, unless indicated otherwise in a credit line to the material. If material is not included in the article's Creative Commons licence and your intended use is not permitted by statutory regulation or exceeds the permitted use, you will need to obtain permission directly from the copyright holder. To view a copy of this licence, visit http://creativecommons.org/licenses/by/4.0/.

those are women [1]. In the absence of preventative therapeutics or a cure, the number of AD sufferers will reach approximately 130 million worldwide by 2050 [2].

AD pathogenesis is estimated to begin decades before symptoms emerge [3, 4]. Biomarkers that track the early pathogenic changes may provide an optimal therapeutic window by identifying those at risk of AD before irreversible brain damage and cognitive impairment occurs. Evidence from preclinical models and at-risk patients suggests the earliest biochemical changes in the AD brain involve glucose hypometabolism and reduced oxygen flow [5, 6], oxidative stress [7–12], inflammation [13], and aberrant processing of amyloid precursor protein (APP) and tau [14–17]. Interestingly, each of these key changes has been linked to mitochondrial dysfunction and the production of reactive oxygen species (ROS) [18, 19]. Mitochondrial function begins to decline during middle age [20], which may underlie the maternally inherited pattern of glucose hypometabolism in the at-risk AD brain [6, 19, 21, 22]. Impaired mitochondria use ROS to alert the cellular environment of impending bioenergetic stress [23]. ROS refers to a family of partially reduced oxygen species, such as $O_2^{\bullet-}$, $HO^{\bullet}$, H_2O_2, NO, and $ONOO^-$, that possess highly reactive properties. ROS directly activate microglia, the resident macrophages of the brain. Activated microglia in turn produce more ROS via NADPH oxidase (NOX) and nitric oxide synthase (NOS) [24, 25]. When the resulting rise in ROS production overwhelms the modest level of endogenous antioxidants in the aging brain, oxidative stress ensues. Oxidative stress modifies the enzymes responsible for pathogenic processing of APP and tau, leading to Aβ and tau accumulation [18]. Aβ and tau, along with oxidized lipids and DNA, can shift microglia into a chronic, ROS-generating phenotype [23, 25–32], thereby propelling the at-risk AD brain into a pro-inflammatory state that is neurotoxic. The primary ROS produced by mitochondria and activated microglia is superoxide ($O_2^{\bullet-}$). Thus, $O_2^{\bullet-}$ provides a signal of mitochondrial and immune (mito-immune) stress, which may be used to track neuroinflammation throughout the course of AD.

Our group has pioneered the development of positron emission tomography (PET) radiotracers for imaging oxidative stress in vivo [33, 34]. The parent compound for radiotracer development is dihydroethidium (DHE), which is primarily oxidized by $O_2^{\bullet-}$ to ethidium and trapped in tissues [35]. Prior validation of [^{18}F]ROStrace demonstrates that it behaves similarly to DHE. Importantly, only the neutral species of [^{18}F]ROStrace crosses the blood brain barrier. Once in the brain, if [^{18}F]ROStrace is oxidized, [^{18}F]*ox*-ROStrace becomes trapped (Fig. 1a). This trapping mechanism results in increased [^{18}F]ROStrace retention in conditions of increased oxidative stress and neuroinflammation [34].

The two major goals of the current study were to determine if [^{18}F]ROStrace is sensitive enough (1) to detect increased oxidative stress in a preclinical model of AD and (2) to predict the accelerated AD pathology in the female brain. Increased amyloid beta (Aβ) is reported to be the earliest neuropathological change in the at-risk AD brain, and the presence of Aβ is currently required for AD diagnosis [36, 37]. We therefore analyzed the relationship of [^{18}F]ROStrace and Aβ in the well-characterized, double-transgenic APP_{SWE}/PS1dE9 (APP/PS1) mouse model. Much like AD patients, Aβ plaques, neuroinflammation, and cognitive defects are more prevalent in female compared to male APP/PS1 mice [38–40]. Due to the established role of oxidative stress in Aβ pathology, we hypothesized that [^{18}F]ROStrace retention would correlate with increased Aβ burden in female APP/PS1 mice. To test this hypothesis, a series of PET imaging studies were conducted in wild-type (WT) and APP/PS1 mice of both sexes at 3 different time points, representing early (5 mo.), middle (10 mo.), and advanced (16 mo.) life. The results of our study show that [^{18}F]ROStrace is increased in the APP/PS1 brain compared to WT. Further, [^{18}F]ROStrace retention is higher and occurs earlier in female APP/PS1 mice. Thus, female AD mice are more prone to oxidative stress than males, and this difference emerges with increased Aβ burden midlife. Our results suggest that differences in oxidative stress during this crucial time may partially explain the sexual dimorphism in AD.

Results

[^{18}F]ROStrace retention is increased in APP/PS1 mice in vivo and reveals a female sex bias

Oxidative stress is a driver of AD pathology in APP/PS1 mice [41, 42]. To determine the sensitivity of [^{18}F]ROStrace to detect increased oxidative stress during the course of AD, a series of micro-PET imaging studies were performed in WT and APP/PS1 mice at 5 mo., 10 mo., and 16 mo. of age (Additional file 1: Fig. S1). Due to the lack of blood sample collection to perform absolute quantitation on [^{18}F]ROStrace PET images and differences in body weight between female and male (Fig. 1b), we utilized a semiquantitative approach based on normalization to a reference region. However, since ROS produced by mitochondria or activated microglia could be throughout the brain, there is no true reference region for quantitating [^{18}F]ROStrace images. Studies of TSPO neuroinflammatory PET imaging agents have suggested using a pseudo-reference region, which is a region of interest (ROI) that has no difference in standardized uptake values (SUVs) among the study groups, to increase the sensitivity of the PET image analysis [43,

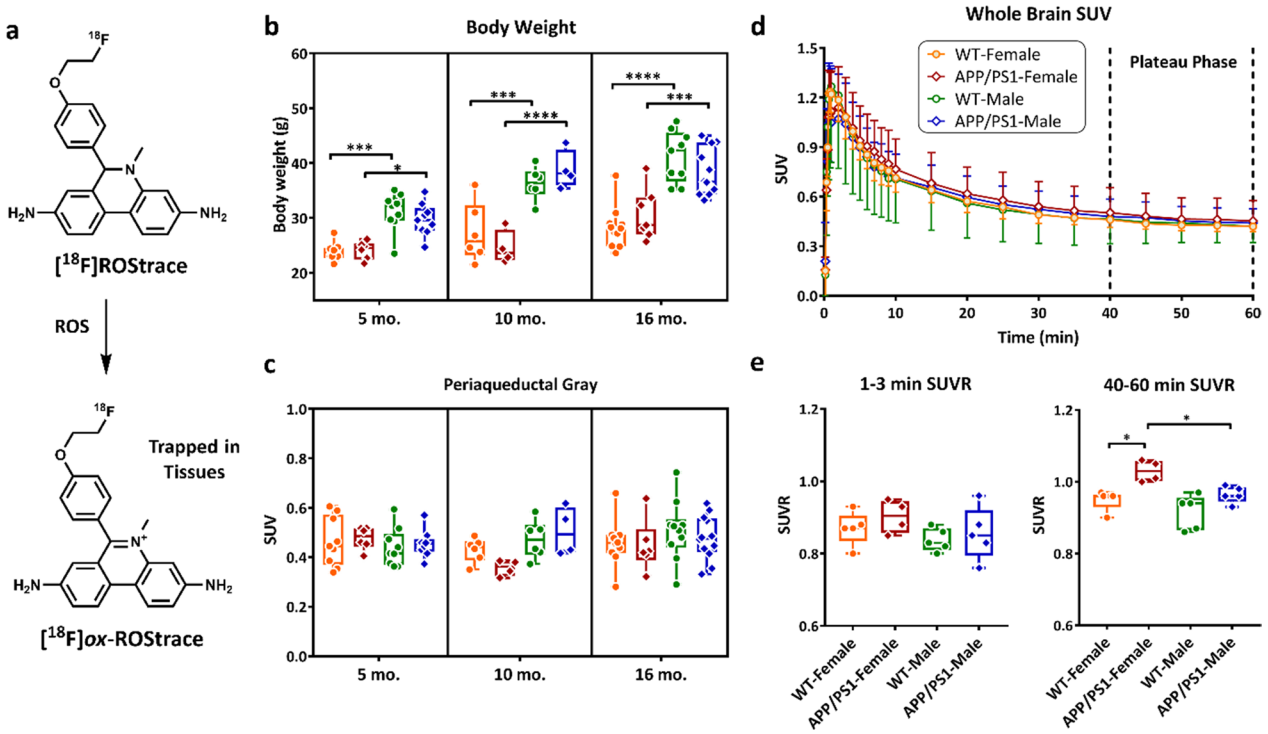

Fig. 1 Validation of the plateau phase and pseudo-reference region for ox[^{18}F]ROStrace PET analysis. **a** The chemical structures of [^{18}F]ROStrace and [^{18}F]*ox*-ROStrace. Comparison of **b** body weight (g) and **c** periaqueductal gray (PAG) SUV from 40–60 min. 5 mo. old: APP/PS1 group: $n=6$ for female, and $n=9$ for male; WT group: $n=9$ per gender,10 mo. old: APP/PS1 group: $n=4$ per gender; WT group: $n=6$ per gender, and 16 mo. old: APP/PS1 group: $n=6$ for female, and $n=12$ for male; WT group: $n=10$ per gender. The statistical significance of p value calculated by two-way ANOVA: ****$p<0.0001$, ***$p<0.001$, *$p<0.05$. Micro-PET data analysis validates that oxidative stress, not blood flow, contributes the [^{18}F]ROStrace signals in the animal brain. Time–activity curves in SUV of whole brain **d** in WT female ($n=5$), WT male ($n=5$), APP/PS1 female ($n=4$), and APP/PS1 male ($n=5$) mice at 16 mo. of age. Data are shown as mean ± standard deviation. Comparison of the average [^{18}F]ROStrace SUVR from 9 VOIs at 16-mo.-old animals in **e** perfusion phase (1–3 min) and plateau phase (40–60 min). (WT groups: $n=5$ per gender, and APP/PS1 group: $n=4$ for female, and $n=5$ for male) The statistical significance of p value calculated by one-way ANOVA (*$p<0.05$)

44]. In the current study, the periaqueductal gray (PAG) was the ROI showing no statistical differences in the [^{18}F]ROStrace SUVs among WT and APP/PS1 in both genders at all ages (Fig. 1c). Therefore, this ROI was selected as the pseudo-reference region for [^{18}F]ROStrace SUV ratio (SUVR) measurement in this preclinical AD study.

First, whole brain time–activity curves were generated from dynamic scans taken 0–60 min post-injection of [^{18}F]ROStrace (Fig. 1d). As previously reported [34], [^{18}F]ROStrace reached peak uptake in brain within 2 min, followed by a washout period for approximately 20 min, and then remained steady in a plateau phase throughout the remainder of the scan. There were no differences in SUVRs during the perfusion phase (1–3 min; Fig. 1e), indicating that [^{18}F]ROStrace levels during the plateau phase, which represent oxidized [^{18}F]ROStrace [34], cannot be attributed to differences in blood flow (Fig. 1e).

Next, regional semi-quantitation SUVR of the plateau phase (40–60 min post-injection; $SUVR_{40-60}$) was calculated for WT and APP/PS1 mice at the three different time points (Fig. 2). Representative micro-PET images of region-specific [^{18}F]ROStrace retention for each strain, age, and sex are shown in Fig. 3. To confirm our micro-PET results, [^{18}F]ROStrace activity was also measured using ex vivo autoradiography (ARG) (Fig. 3). [^{18}F]ROStrace retention was indistinguishable among all brain regions of the APP/PS1 and WT mice at the earliest time point of 5 mo. (Fig. 2a). [^{18}F]ROStrace retention was higher in the cortex and cerebellum of the APP/PS1 females compared to APP/PS1 males ($p<0.05$; Additional file 1: Table S1). This sex-based difference was amplified at 10 mo. of age, where APP/PS1 females demonstrated increased [^{18}F]ROStrace retention over that of APP/PS1 males in every brain region except the midbrain and brainstem (Fig. 2b). Compared to WT mice, [^{18}F]ROStrace retention was increased in the cortex ($p=0.0002$), striatum ($p=0.0116$), hippocampus ($p=0.0336$), and amygdala ($p=0.0010$) of female APP/PPS1, whereas APP/PS1 males remained indistinguishable from WT (Fig. 2b).

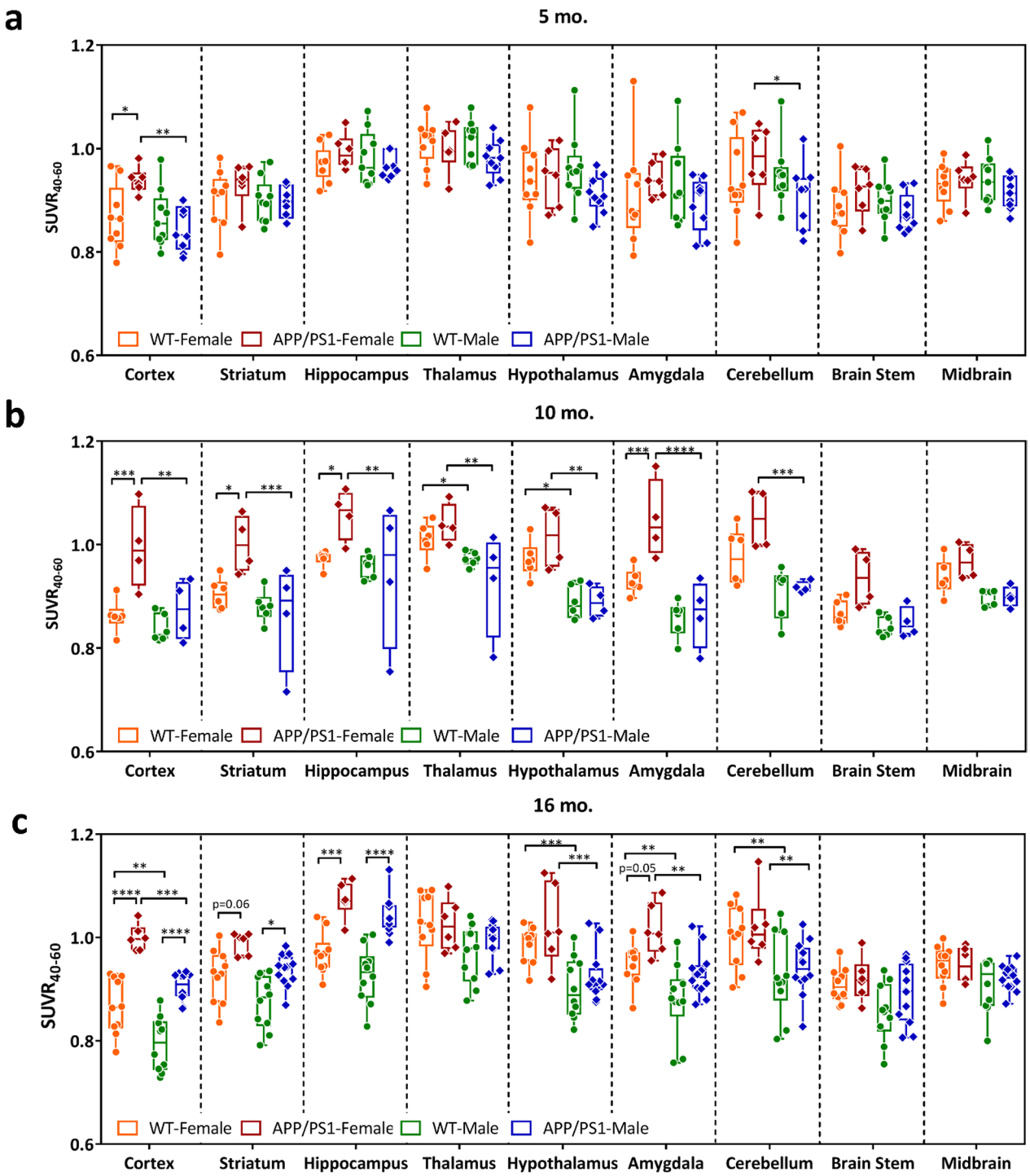

Fig. 2 Regional differences in [^{18}F]ROStrace uptake from 9 VOIs presented as standard uptake value ratios from 40–60 min post-injection ($SUVR_{40\text{-}60}$) in WT and APP/PS1 mice at **a** 5 mo. old: APP/PS1 group: $n=6$ for female, and $n=9$ for male; WT group: $n=9$ per gender, **b** 10 mo. old: APP/PS1 group: $n=4$ per gender; WT group: $n=6$ per gender, and **c** 16 mo. old: APP/PS1 group: $n=6$ for female, and $n=12$ for male; WT group: $n=10$ per gender. The statistical significance of p value calculated by two-way ANOVA (*$p<0.05$, **$p<0.01$, ***$p<0.001$, ****$p<0.0001$)

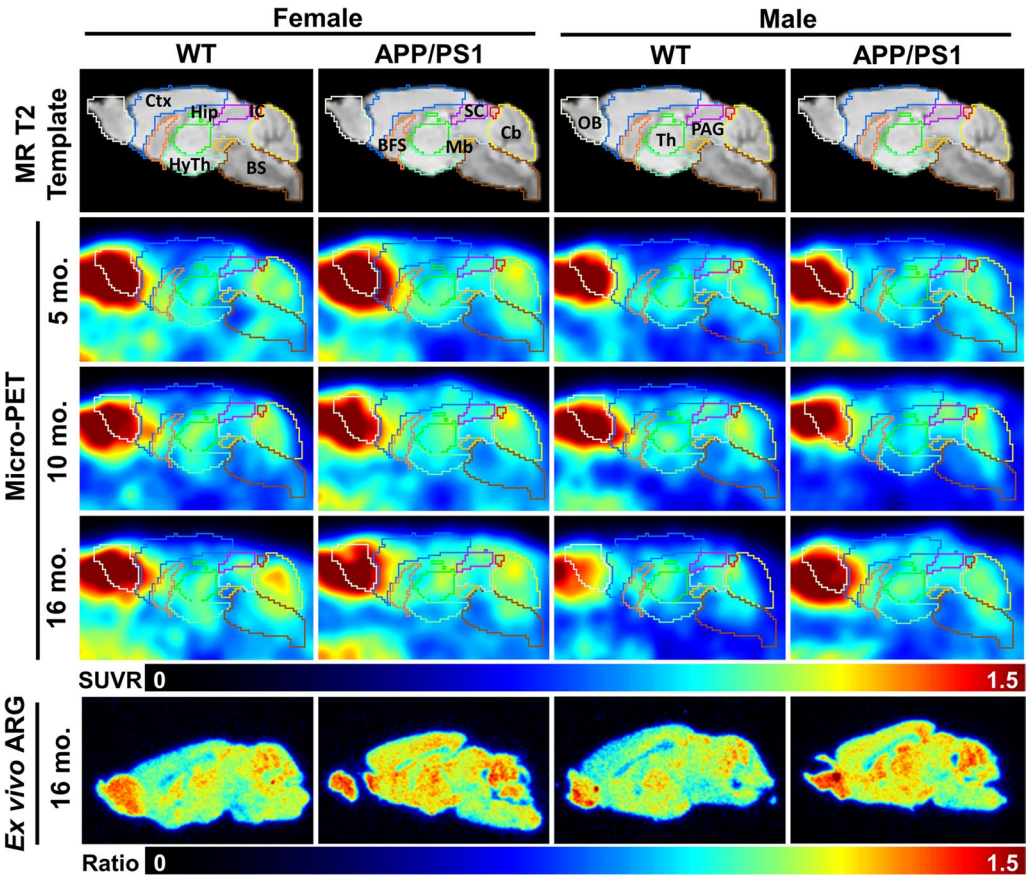

Fig. 3 In vivo [^{18}F]ROStrace retention is increased in the APP/PS1 model of AD and demonstrates a female sex bias. Sagittal view of [^{18}F]ROStrace $SUVR_{40\text{-}60}$ PET images collected from both sexes of WT and APP/PS1 mice at 5 mo., 10 mo., and 16 mo. Brain subregions derived from Mirrione mouse brain atlas. Ctx: cortex, OB; olfactory bulb, BFS: basal forebrain septum, Hip: hippocampus, HyTh: hypothalamus, SC: superior colliculi, IC: inferior colliculi, Cb: cerebellum, BS: brain stem, Th: thalamus, PAG: periaqueductal gray, and Mb: midbrain

The pattern of increased [^{18}F]ROStrace retention in female APP/PS1 versus WT was similar at 10 and 16 mo. of age, but augmented in the cortex ($p < 0.0001$) and hippocampus ($p = 0.0003$) over time (Fig. 2c, Additional file 1: Table S1). Finally, at 16 mo. of age, [^{18}F]ROStrace retention increased in APP/PS1 male mice. Higher $SUVR_{40-60}$ levels were observed in APP/PS1 versus WT male in cortex ($p < 0.0001$), striatum ($p = 0.0183$), and hippocampus ($p < 0.0001$) (Fig. 2c). Differential [^{18}F]ROStrace retention in female *vs.* male WT mice began in the hypothalamus at mid-life ($p = 0.0156$), and spread to the cortex ($p = 0.0055$), amygdala ($p = 0.0006$), and cerebellum ($p = 0.004$) in advanced life.

In order to understand the effect of aging on retention of [^{18}F]ROStrace in brain tissue, $SUVR_{40-60}$ measurements were compared within female and male WT and APP/PS1 mice over time using a two-way ANOVA. The statistical comparisons show a decrease in several regions in male WT mice from 5 to 16 mo., but [^{18}F]ROStrace remained stable in most regions of the WT female brain over time (Additional file 1: Table S1). Conversely, [^{18}F]ROStrace retention increased over time in mice with APP/PS1 mutations, regardless of sex. From 5 to 16 mo., [^{18}F]ROStrace retention increased in the hippocampus ($p = 0.0126$) and hypothalamus ($p = 0.0377$) of APP/PS1 females, but only the hippocampus ($p = 0.0002$) of APP/PS1 males.

[^{18}F]ROStrace retention correlates with APP/PS1 amyloid burden

ROS induce Aβ-generating β- and γ-secretases [45], while inhibiting Aβ-clearing enzymes [46]. The resulting Aβ aggregates are associated with activated microglia and oxidative damage in the AD brain. Therefore, we hypothesized that [^{18}F]ROStrace levels would correlate with Aβ burden in APP/PS1 mice in a region-specific manner. To test this hypothesis, statistical parametric mapping (SPM) was first used to distinguish brain regions with elevated ROS in APP/PS1 relative to WT in both sexes

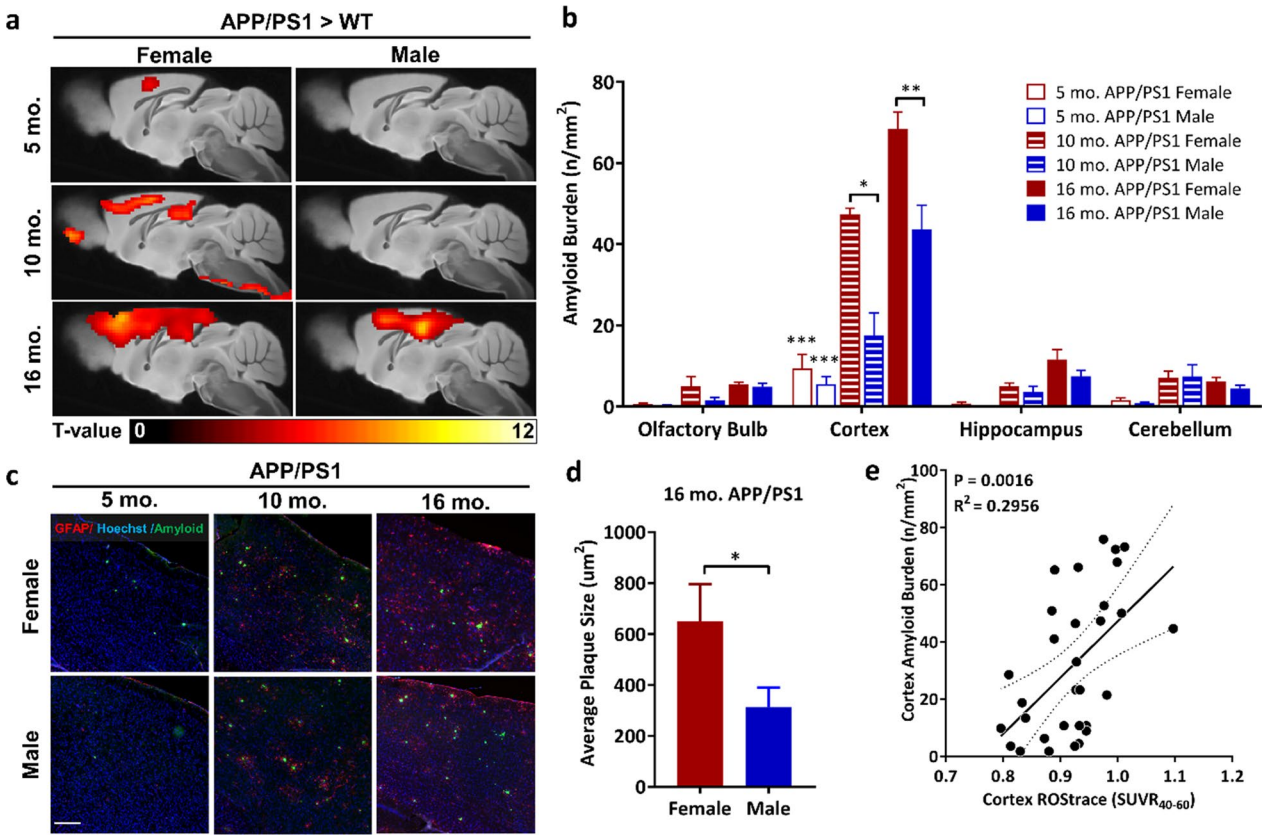

Fig. 4 Elevated [^{18}F]ROStrace retention in the APP/PS1 brain maps with spatial distribution of amyloid deposits and positively correlates with increased amyloid burden in the cortex of aging APP/PS1 mouse brain. **a** Statistical parametric mapping (SPM) analysis showing significant differences (uncorrected $p < 0.005$ and an extent cluster threshold = 50) in [^{18}F]ROStrace retention per sex in 5 mo. (top row), 10 mo. (middle row), and 16 mo. (bottom row) APP/PS1 mice versus WT. **b** Quantification of amyloid burden in 4 different brain regions of the APP/PS1 female (red) and male (blue) mouse brain. 5 mo. old APP/PS1 group: $n = 9$ for male, $n = 5$ for female, 10 mo. old APP/PS1 group: $n = 4$ per gender. 16 mo. old APP/PS1 group: $n = 8$ for male, $n = 5$ for female. The statistical significance calculated by two-way ANOVA. *$p < 0.05$, **$p < 0.005$. ***$p < 0.0001$, relative to olfactory bulb, hippocampus, and cerebellum at 5-mo.-old APP/PS1 mouse. Values represent mean ± SEM. **c** Images of the cortex region of APP/PS1 mice 5–16 mo. of age stained with anti-GFAP (red), anti-beta amyloid 1–42 antibodies (green) and Hoechst (blue). Scale bar = 150 µm. **d** Average size of amyloid plaques in the cortex region of brains collected from 16-mo.-old APP/PS1 mice, $n = 8$ for male, $n = 5$ for female. The statistical significance of p value calculated by unpaired *t* test. Values represent mean ± SEM. *$p < 0.05$ **e** Linear regression analysis of cortical amyloid burden (n/mm^2) and [^{18}F]ROStrace SUVR$_{40\text{-}60}$

(Fig. 4a). The SPM results show elevation of [^{18}F]ROStrace retention in APP/PS1 female mice at 10 mo. of age in hippocampus and cortex. By 16 mo., [^{18}F]ROStrace levels were augmented and extended to broader areas of both regions (Fig. 4a). In APP/PS1 males, higher [^{18}F]ROStrace was also observed in the hippocampus and cortex, but only at the most advanced age.

Next, the brains from 5-, 10-, and 16-mo.-old APP/PS1 mice were processed with anti-amyloid and glial fibrillary acidic protein (GFAP) antibodies. During pro-inflammatory conditions like trauma and amyloidosis, astrocytes assist in neuronal repair by creating a barrier to confine toxic elements and pave the way for microglial phagocytosis [47]. Our co-staining results confirm that amyloid plaques were closely surrounded by GFAP-positive astrocytes in the APP/PS1 brain. The representative images in Additional file 1: Fig. S2 show that very few Aβ aggregates were visible at 5 mo. of age in either sex, and these were predominately found in the olfactory bulb and the cortex. Female APP/PS1 mice also had sparse, small Aβ aggregates in the cerebellum at 5 mo. By 10 mo. of age, Aβ aggregates were detected throughout all four brain regions (olfactory bulb, cortex, hippocampus, and cerebellum), but were most prevalent in the cortex and hippocampus. A similar trend of Aβ distribution was seen at 16 mo.

To further investigate the relationship between regional amyloid burden and [^{18}F]ROStrace, low magnification images of sagittal brain sections were acquired from APP/PS1 mice in each age group and the number of amyloid

aggregates quantified in 4 key regions (Fig. 4b, Additional file 1: Fig. S2). The results show that the cortex is not only the first brain region where significant amyloid plaques appeared ($p < 0.0001$ for cortex *vs.* olfactory bulb, hippocampus, and cerebellum at 5 mo.), but also the region that bore the heaviest amyloid burden with increasing age (Fig. 4b, c). Amyloid burden in the cortex was higher in APP/PS1 females than in age-matched males, which became significant at 10 mo. (Fig. 4b). The size of amyloid plaques was also largest in the cortex of APP/PS1 female mice at 16 mo. (Fig. 4d). These results confirm previous reports of increased Aβ burden in APP/PS1 females [38, 39]. Interestingly, the cortex was also the first region to show increased [^{18}F]ROStrace levels in both sexes of APP/PS1 mice, and [^{18}F]ROStrace remained consistently higher in the APP/PS1 female *vs.* male cortex over time. To evaluate the significance of this association, linear regression analysis was performed for amyloid burden versus [^{18}F]ROStrace $SUVR_{40-60}$ in the cortex of APP/PS1 mice, which revealed a positive correlation between amyloid burden and [^{18}F]ROStrace ($p = 0.0016$, $R^2 = 0.30$; Fig. 4e). Collectively, these results highlight the sensitivity of [^{18}F]ROStrace to predict AD progression.

Validation of increased oxidative stress in the APP/PS1 brain

We further characterized the oxidative stress detected by [^{18}F]ROStrace in vivo by analyzing the same brains with established fluorescent detection methods. Following the PET scan, mice were injected with the parent compound, DHE (5 mg/kg, i.p.) and euthanized 30 min later. To estimate the cellular source of the [^{18}F]ROStrace signal, colocalization between DHE and three major brain cell types was then determined using cell-type specific markers for neurons (NeuN), microglia (IBA-1), and astrocytes (GFAP) (Fig. 5). The fluorescent images revealed that DHE was localized to the cytoplasm of neurons in the APP/PS1 brain only (Fig. 5a, b), which may represent Aβ-induced mitochondrial ROS [12, 48]. DHE was also frequently found in aggregated microglia in the APP/PS1 brain. These aggregated microglia surrounded amyloid plaques and had an amoeboid shape, with a large cell body and relatively few, short processes, resembling an activated morphology (Fig. 5d). In contrast, DHE was rarely detected in the microglia of age-matched WT brain (Fig. 5c). Lastly, DHE signal showed no detectable colocalization with GFAP, indicating that astrocytes have

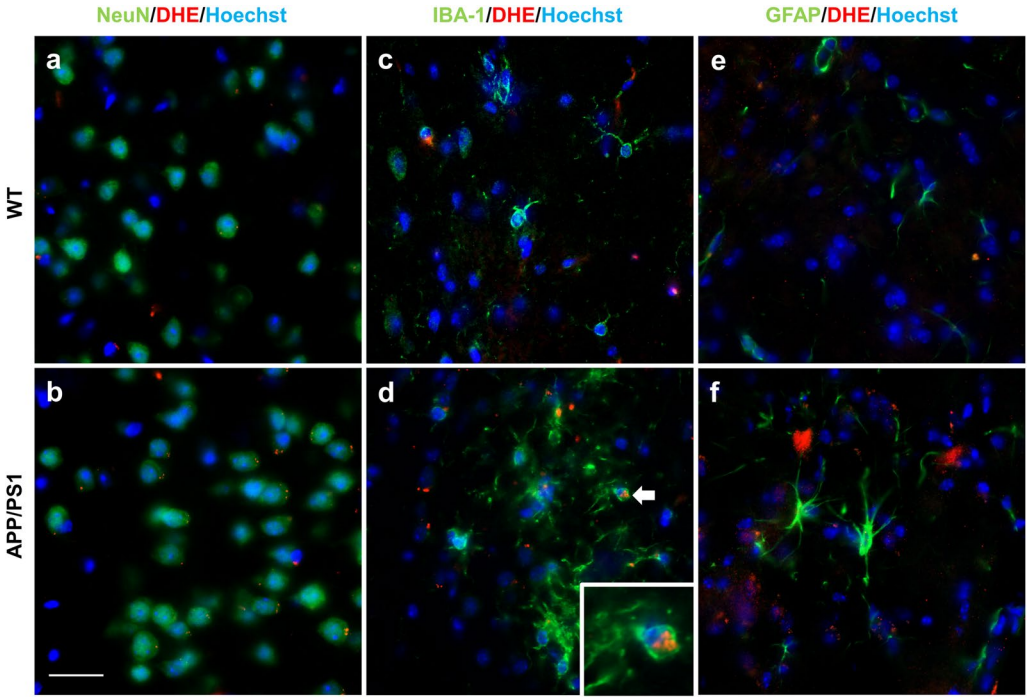

Fig. 5 DHE colocalizes with microglia and neurons, but not astrocytes, in the APP/PS1 brain. Representative confocal micrographs showing colocalization of **a, b** oxidized DHE (red) with neurons (NeuN; green) and **c, d** microglia (IBA-1; green) in WT and APP/PS1 cortex. **e, f** Oxidized DHE did not colocalize with astrocytes (GFAP, green). The inlet is a magnified region of that indicated by the white arrow. Scale bar = 20 μm

minimal involvement in the ROS signal detected by DHE (Fig. 5e, f), and presumably [^{18}F]ROStrace, in both WT and APP/PS1 animals.

One of the key mediators of ROS-induced neurotoxicity in AD is peroxynitrite, ($ONOO^-$) [49, 50]. $ONOO^-$ is a powerful oxidant produced by O_2^- and nitric oxide ($^{\bullet}NO$) that permanently alters proteins via nitration of tyrosine residues. To determine the relationship between $O_2^{\bullet-}$ detected by [^{18}F]ROStrace and downstream oxidative damage, we quantified levels of 3-nitrotryosine (3NT) in age-matched WT and APP/PS1 mouse brains using IHC. A gradual elevation of 3NT was observed in the cortex of aging APP/PS1 mouse brain (Additional file 1: Fig. S3), which only became significant at 16 mo. of age (Fig. 6a). As expected, APP/PS1 females suffered the most extensive oxidative damage, evidenced by the highest number of 3NT-positive cells (Fig. 6b).

Discussion

The preclinical studies described herein suggest that oxidative stress may contribute to the increased risk of AD in women. Using the novel superoxide sensitive PET tracer, [^{18}F]ROStrace, we detected increased oxidative stress in the female AD brain in vivo, which coincided with increased Aβ and preceded the accumulation of neuronal damage. Increased Aβ is one of the earliest neuropathological changes in the at-risk AD brain and is required for AD diagnosis [36, 37]. However, the disconnect between Aβ and cognitive performance presents a major limitation and suggests additional biomarkers are needed to predict the progression of neurodegeneration and gauge therapeutic efficacy throughout the course of disease [51]. Our results suggest [^{18}F]ROStrace is a promising tool to bridge this gap.

Mitochondrial dysfunction and microglial activation occur early in the neurodegeneration process, leading to a collective increase in ROS production and oxidative stress that continues through the course of AD. Markers of oxidative damage have been reported in mild cognitive impairment and early AD, but longitudinal analysis has thus far been limited to biofluids. Herein, we confirm the early and persistent role of oxidative stress in the brain using [^{18}F]ROStrace PET. We found that the fluorescent parent compound of [^{18}F]ROStrace, DHE, colocalized to neurons and microglia in the AD brain. These observations are in line with prior studies describing increased production of $O_2^{\bullet-}$ by neuronal mitochondria and activated microglia in response to Aβ [12, 32, 52, 53]. In addition to $O_2^{\bullet-}$, Aβ also induces $^{\bullet}NO$ in both mitochondria and microglia [54, 55]. $^{\bullet}NO$ is the only molecule that can out-compete superoxide dismutase for $O_2^{\bullet-}$, reacting with $O_2^{\bullet-}$ at an estimated rate of $4–16 \times 10^9\ M^{-1}\ s^{-1}$ to

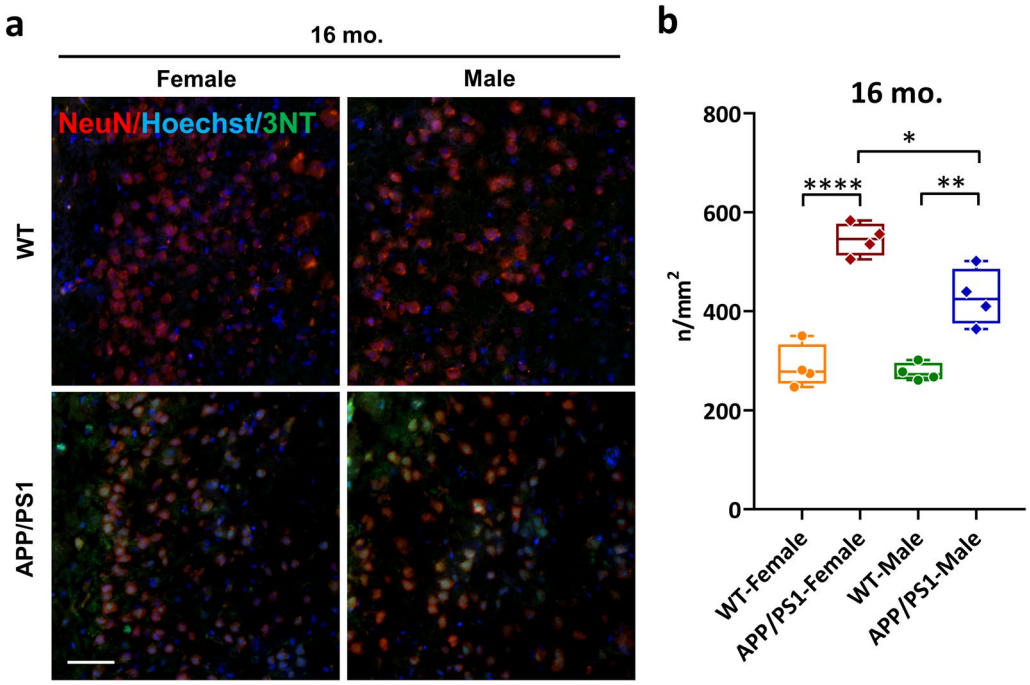

Fig. 6 Oxidative damage is highest in the female APP/PS1 at advanced age. **a** Representative confocal images showing increased oxidative damage in neurons (NeuN; red) of APP/PS1 mice detected by 3-nitrotyrosine (3NT; green) adducts in the cortex at 16 mo. of age. Scale bar = 50 μm. **b** Quantification of 3NT-positive cells in the cortex of age-matched WT and APP/PS1 mouse brain tissues, $n = 4$ per group. The statistical significance of p value calculated by one-way ANOVA. Values represent mean ± SEM, *$p < 0.05$, **$p < 0.005$, ****$p < 0.0001$

form peroxynitrite, $ONOO^-$ [56, 57]. $ONOO^-$ permanently modifies proteins by nitrating tyrosine residues, which can thus be used as a molecular footprint of oxidative damage [58]. Using 3-nitrotyrosine, we found oxidative damage increased over time in the AD brain, as expected [49, 50], but was highest in females. Notably, the increase in [^{18}F]ROStrace retention preceded oxidative damage in neurons, suggesting [^{18}F]ROStrace may serve as a predictive biomarker of downstream neuronal demise.

The mito-immune shifts that occur in the female brain due to estrogen changes midlife are thought to be a major contributor to the increased risk of females to AD [59]. We selected 3 time points for [^{18}F]ROStrace imaging that, for female mice, represent key states which closely resemble the human condition during premenopause (5 mo.), perimenopause (10 mo.), and postmenopause (16 mo.) [60–62]. Interestingly, a significant difference in [^{18}F]ROStrace retention in WT females and males was observed in hypothalamus. The hypothalamus plays an important role of neuroendocrine function, especially in regulating estrogen in females [63–66]. The hypothalamic increase in [^{18}F]ROStrace retention in females began at 10 mo., which represents the midpoint of the proposed perimenopausal phase (7–12 mo.) in mice [61, 62]. Perimenopause describes the midlife transition to reproductive senescence.

Perimenopause also represents a critical transition period in the aging female brain, requiring metabolic adaptation to the decline in estrogen-dependent bioenergetics [63]. Most women maintain the neurological resilience to transition through perimenopause without long-term consequences. However, for those at risk of AD, the neurological challenges involved in perimenopause may overwhelm the system and tip the scales toward neurodegeneration. Our results suggest that oxidative stress is a key indicator of this proposed tipping point.

Estrogen regulates mitochondrial biogenesis [67, 68], endogenous antioxidants [69], and microglial activation [40, 70]. Thus, in an environment of increased Aβ, such as the APP/PS1 brain, a decline in estrogen signaling would act as a second hit on mitochondrial function, leading to increased ROS production [71]. Increased mitochondrial ROS can drive the conversion of microglia into a pro-inflammatory phenotype by impairing oxidative phosphorylation, inducing mitochondrial fission, activating nuclear factor kappa B (NF-kB), and stimulating the metabolic switch to glycolysis [72]. Pro-inflammatory microglia amplify ROS production, which can become neurotoxic. Microglia in the female AD brain are predominately pro-inflammatory and less phagocytic than that of males, leading to increased amyloid burden and oxidative stress [40]. In preclinical models, oxidative stress induces every established pathological hallmark of AD [18]. Therefore, increased oxidative stress in the brain during midlife, when AD-related neurodegeneration is proposed to begin, may serve as a predictive biomarker of AD pathogenesis. Future studies are required to determine the underlying mechanisms responsible for increased oxidative stress in females, and whether beta-estradiol or other antioxidant therapy administered during this critical, early phase may prevent oxidative stress and slow AD progression in at-risk patients.

Conclusions

The current study demonstrates that the signal of [^{18}F]ROStrace is significantly increased in APP/PS1 mouse brain compared to age-matched WT controls. The high retention of [^{18}F]ROStrace also correlates with Aβ burden in cortex of aged APP/PS1 mouse brain. IHC analysis reveals that activated microglia and oxidative stress in neurons are the main contributors for the high [^{18}F]ROStrace signal in APP/PS1 mouse brain. Furthermore, [^{18}F]ROStrace retention is highest and occurs earlier in female APP/PS1 mice, peaking midlife during the perimenopausal phase. [^{18}F]ROStrace may also provide a long-awaited tool to stratify at-risk patients who may benefit from antioxidant therapy prior to irreparable neurodegeneration.

Materials and Methods

Animal models and experimental scheme

All animal experiments in this study were performed under protocols approved by the University of Pennsylvania Institutional Animal Care and Use Committee (IACUC). The double-transgenic APP_{SWE}/PS1dE9 (APP/PS1) mice expressing Mo/HuAPP695swe (chimeric mouse and human amyloid precursor protein) and PS1dE9 (mutant human presenilin 1) and the littermate control C57Bl/6J (WT; wild type) were purchased from Mutant Mouse Resource and Research Center (MMRRC). A total of 91 mice including 41 APP/PS1 (5 mo.: 6 female and 9 male; 10 mo.: 4 female and 4 male; 16 mo.: 6 female and 12 male) and 50 WT (5 mo.: 9 female and 9 male; 10 mo.: 6 female and 6 male; 16 mo.: 10 female and 10 male) were used in this study. The general experimental scheme of this study is shown in Additional file 1: Fig. S1. Briefly, animals selected from each age group received 7.4–11.1 MBq of [^{18}F]ROStrace via tail vein injection. After a 20 min (40–60 min post-injection) or a one hour (0–60 min post-injection) dynamic PET scan, a dose of 5 mg/kg DHE (Sigma-Aldrich, St. Louis, MO, USA) was injected to the animals. The animals were killed 30 min after DHE injection, and brains were extracted for subsequent experiments.

Preparation of [^{18}F]ROStrace

The radiosynthesis of [^{18}F]ROStrace was prepared as previously described [34]. Briefly, [^{18}F]ROStrace was accomplished on all-in-One module (Trasis, Belgium) with full automation. The final product was diluted with 0.6 mL of ethanol, 0.1% ascorbic acid, and 6 mL normal saline and filtered by 0.2 μM nylon filter. The radiochemical yield was 4–20%, and the specific activity was 74 GBq/μmol.

Micro-PET imaging

PET imaging was performed on the β-Cube PET scanner (Molecubes, Ghent, Belgium). The body weight of each animal was measured before the PET scan (Fig. 1b). Animals were anesthetized with 1–2% isoflurane, a tail vein catheter was placed for PET tracer administration, and the animal was placed on the scanner bed. Dynamic scans of 0–60 min or 40–60 min post-injection were acquired after injection of 7.4–11.1 MBq of [^{18}F]ROStrace. After completion of the PET scan, the animal was transferred to the X-Cube CT scanner (Molecubes, Ghent, Belgium) and a general-purpose CT scan was acquired for anatomical reference and attenuation correction. PET images were reconstructed with a matrix size of $192 \times 192 \times 384$, and a voxel size of $0.4 \times 0.4 \times 0.4$ mm with frame lengths of 6×10 s, 9×60 s, and 10×300 s for 60 min dynamic scans or 4×300 s for 20 min scans. All corrections were applied using a manufacturer supplied reconstruction program. CT images were reconstructed with a matrix size of $200 \times 200 \times 550$, and a voxel size of $0.2 \times 0.2 \times 0.2$ mm with a manufacturer supplied reconstruction program.

Micro-PET image analysis

All the [^{18}F]ROStrace micro-PET/CT imaging data were processed and analyzed by using Pmod software (version 3.7, PMOD Technologies Ltd., Zurich, Switzerland). Rigid body matching was manually performed on individual micro-CT images to co-register to the Mirrione mouse MR-T2 weighted brain template [73]. Then, the resulting transformation parameters were applied to the corresponding micro-PET image. Ten volumes of interest (VOIs) including cortex, thalamus, cerebellum, hypothalamus, brain stem, periaqueductal gray, striatum, hippocampus, amygdala, and midbrain were selected from the Mirrione atlas [73]. Due to the lack of the blood samples to perform absolute quantitation and a true reference region to semi-quantitate neuroinflammation images, a pseudo-reference region [44] is needed for [^{18}F]ROStrace neuroinflammation imaging evaluation. Therefore, the periaqueductal gray, with no significant difference in standardized uptake values (SUVs; Fig. 1b) among the different animal groups, was selected as the pseudo-reference region for calculating the SUV ratio (SUVR) for each VOI. The 1–3 min SUVR and the 40–60 min SUVR ($SUVR_{40\text{-}60}$) were extracted from all the VOIs for the perfusion and the late phase comparison from the nineteen 16-mo.-old animals (5 WT female, 5 WT male, 4 APP/PS1 female, and 5 APP/PS1 male) with 1 h full dynamic [^{18}F]ROStrace imaging.

Voxel-wise analyses were performed by using Statistical Parametric Mapping 12 (SPM12, Welcome Department of Cognitive Neurology, Institute of Neurology, London, UK; https://www.fil.ion.ucl.ac.uk/spm) and carried out with the SPMMouse (http://www.spmmouse.org/) [74] animal brain toolbox implemented in MATLAB R2017b (MathWorks Inc., Natick, MA). A voxel-wise two-sample t test was used to compare the [^{18}F]ROStrace $SUVR_{40\text{-}60}$ parametric images between WT and APP/PS1 in each age group (5, 10, and 16 mo.) for both female and male. Due to the small sample size of the studies, the SPMMouse analyses were evaluated by using a relative stringent threshold of a p value < 0.005 with uncorrected statistic and a voxel extent of 50.

Ex vivo autoradiography (ARG)

Mouse brains were collected immediately after [^{18}F]ROStrace micro-PET scan completion. The mouse brains were frozen and sectioned sagittally with a thickness of 30 μm on a cryostat (Leica Biosystems, Germany), and then, the tissue slides were air-dried for next step. The slides were exposed to phosphor plates (BAS 2040, GE Healthcare, Chicago, IL, USA) for 1 day, and the ARG images were digitized by the Typhoon FLA 7000 (West Avenue, Stamford, USA). The ARG images were analyzed by using Pmod software. The ROI of periaqueductal gray was manually delineated for further calculating the ratio of images relative to it.

Immunohistochemical (IHC) analysis

Collected brain tissues were embedded with Tissue-Tek optimal cutting temperature (Sakura, Japan) and frozen and then cut into 12 μm sagittal sections. The brain sections were fixed with 4% paraformaldehyde (PFA) at room temperature before staining and then rinsed with phosphate buffered saline (PBS). Then, 15 min of 0.1% Triton X-100 in PBS was applied to permeabilized tissues. After rinse with PBS, brain sections were blocked with 10% bovine serum albumin (BSA) for 1 h at room temperature. Selected slides were incubated with primary antibodies (Additional file 1: Table S2) overnight at 4 °C. The following day, after wash with 1% BSA in PBS, slides were incubated with corresponding secondary antibodies (Additional file 1: Table S2) for 1 h at room temperature. All slides were counterstained with Hoechst (1:2000, PBS, Thermo Fisher Scientific, H3570) and mounted with VectaShield Antifade Mounting Media (Vector

Laboratories, 101098-042). Images were acquired by using Zeiss Axio Observer Microscope and Zeiss 710 Confocal Microscope (Germany). Panoramic brain tissue images were acquired by Keyence BZ-X800 Microscope (Osaka, Japan). For cortex amyloid burden and 3NT-positive cells quantification, images were uploaded onto Fiji software, amyloid plaques and 3NT-positive cells within the ROI (1.73 mm × 0.65 mm) were counted manually by using the cell counter plugin, and quantification results were scaled to n/mm^2. The average plaque sizes of each Aβ plaque in brain were measured by Zen software (Zeiss, Germany).

Statistical analysis

All the statistical analyses were performed on GraphPad Prism software, version 7.02 (GraphPad Inc., San Diego, CA), and the results were presented as mean ± standard error (SEM) or mean ± standard deviation (SD) as noted. The statistical significance between different animal groups was determined either with one-way or two-way ANOVA following Sidak's or Turkey post hoc *t* test. A p value < 0.05 was considered as the threshold of statistically significant.

Abbreviations

AD	Alzheimer's disease
Aβ	Amyloid beta
APP	Amyloid precursor protein
APP/PS1	APPSWE/PS1dE9
ARG	Autoradiography
DHE	Dihydroethidium
GFAP	Glial fibrillary acidic protein
NF-kB	Nuclear factor kappa B
$^{\bullet}$NO	Nitric oxide
NOX	NADPH oxidase
NOS	Nitric oxide synthase
3NT	3-Nitrotryosine
$O_2^{\bullet-}$	Superoxide
$ONOO^-$	Peroxynitrite
PAG	Periaqueductal gray
PET	Positron emission tomography
ROI	Region of interest
ROS	Reactive oxygen species
SPM	Statistical parametric mapping
SUV	Standardized uptake values
SUVR	SUV ratio
$SUVR_{40-60}$	40–60 Min SUVR
VOI	Volume of interest
WT	Wild type

Supplementary Information

The online version contains supplementary material available at https://doi.org/10.1186/s13550-022-00914-x.

Additional file 1: Fig. S1. Schematic illustration of experimental scheme. **Figure S2**. Comparison of amyloid plaques spatial distribution in age-matched APP/PS1 male and female mouse brains. **Figure S3**. Oxidative damage detected by 3NT in neurons over time in WT and APP/PS1 cortex. **Table S1**. Summary of regional $SUVR_{40-60}$ statistical analysis in age- and gender-matched APP/PS1 and WT mice at the age of 5, 10, and 16 mo. **Table S2**. Information of antibodies.

Acknowledgements

We thank Eric Blankemeyer and the University of Pennsylvania Small Animal Imaging Facility for the assistance with micro-PET image studies.

Author contributions

The study was designed by RHM, MJM, CH, YZ, and CJH. Material preparation, data collection, and analysis were performed by CJH, CH, YZ, JYL, NK, EG, KX, HL, and SL. The manuscript was written by MJM, CJH, and RHM. All authors read and approved the final manuscript.

Funding

This research was funded by the National Institutes of Health, National Institute of Aging, grant number AG055142, and the National Institute of Neurological Disorders and Stroke grant number NS114656.

Availability of data and materials

All data generated or analyzed during this study are included in this published article and its supplementary information files.

Declarations

Ethics approval and consent to participate

All procedures performed in studies involving animals were approved by the University of Pennsylvania Institutional Animal Care and Use Committee (IACUC). All methods were carried out in accordance with relevant guidelines and regulations including Animal Research: Reporting of In Vivo Experiments (ARRIVE) guidelines. This article does not contain any studies with human participants performed by any of the authors.

Consent for publication

Not applicable.

Competing interests

The authors declare that they have no competing interests.

Received: 6 June 2022 Accepted: 18 July 2022
Published: 27 July 2022

References

1. Brookmeyer R, Johnson E, Ziegler-Graham K, Arrighi HM. Forecasting the global burden of Alzheimer's disease. Alzheimers Dement. 2007;3:186–91. https://doi.org/10.1016/j.jalz.2007.04.381.
2. Hebert LE, Weuve J, Scherr PA, Evans DA. Alzheimer disease in the United States (2010–2050) estimated using the 2010 census. Neurology. 2013;80:1778–83. https://doi.org/10.1212/WNL.0b013e31828726f5.
3. Bateman RJ, Xiong C, Benzinger TLS, Fagan AM, Goate A, Fox NC, et al. Clinical and biomarker changes in dominantly inherited Alzheimer's disease. N Engl J Med. 2012;367:795–804. https://doi.org/10.1056/NEJMoa1202753.
4. Reitz C, Brayne C, Mayeux R. Epidemiology of Alzheimer disease. Nat Rev Neurol. 2011;7:137–52. https://doi.org/10.1038/nrneurol.2011.2.
5. Wang Y, Shang Y, Mishra A, Bacon E, Yin F, Brinton R. Midlife chronological and endocrinological transitions in brain metabolism: system biology basis for increased Alzheimer's risk in female brain. Sci Rep. 2020;10:8528. https://doi.org/10.1038/s41598-020-65402-5.
6. Mosconi L, Mistur R, Switalski R, Brys M, Glodzik L, Rich K, et al. Declining brain glucose metabolism in normal individuals with a maternal history of Alzheimer disease. Neurology. 2009;72:513–20.
7. Klein JAAS. Oxidative stress, cell cycle, and neurodegeneration. J Clin Invest. 2003;111:785–93. https://doi.org/10.1172/JCI200318182.
8. Mariani E, Polidori MC, Cherubini A, Mecocci P. Oxidative stress in brain aging, neurodegenerative and vascular diseases: an overview. J Chromatogr B Analyt Technol Biomed Life Sci. 2005;827:65–75. https://doi.org/10.1016/j.jchromb.2005.04.023.
9. Huang WJ, Zhang X, Chen WW. Role of oxidative stress in Alzheimer's disease. Biomed Rep. 2016;4:519–22. https://doi.org/10.3892/br.2016.630.

10. TE Tonnies E. Oxidative stress, synaptic dysfunction, and Alzheimer's disease. J Alzheimer's Dis. 2017;57:1105–21. https://doi.org/10.3233/JAD-161088.
11. Cheignon C, Tomas M, Bonnefont-Rousselot D, Faller P, Hureau C, Collin F. Oxidative stress and the amyloid beta peptide in Alzheimer's disease. Redox Biol. 2018;14:450–64. https://doi.org/10.1016/j.redox.2017.10.014.
12. McManus MJ, Murphy MP, Franklin JL. The mitochondria-targeted antioxidant MitoQ prevents loss of spatial memory retention and early neuropathology in a transgenic mouse model of Alzheimer's disease. J Neurosci. 2011;31:15703–15. https://doi.org/10.1523/JNEUROSCI.0552-11.2011.
13. Chung HY, Cesari M, Anton S, Marzetti E, Giovannini S, Seo AY, et al. Molecular inflammation: underpinnings of aging and age-related diseases. Ageing Res Rev. 2009;8:18–30. https://doi.org/10.1016/j.arr.2008.07.002.
14. Lambert MPBAK, Chromy BA, Edwards C, Freed R, Liosatos M, Morgan TE, Rozovsky I, Trommer B, Viola KL, Wals P, Zhang C, Finch CE, Krafft GA, Klein WL. Diffusible, nonfibrillar ligands derived from Abeta1-42 are potent central nervous system neurotoxins. Proc Natl Acad Sci USA. 1998;26:6448–53.
15. Deshpande A, Mina E, Glabe C, Busciglio J. Different conformations of amyloid beta induce neurotoxicity by distinct mechanisms in human cortical neurons. J Neurosci. 2006;26:6011–8. https://doi.org/10.1523/JNEUROSCI.1189-06.2006.
16. Cappai R, Barnham KJ. Delineating the mechanism of Alzheimer's disease A beta peptide neurotoxicity. Neurochem Res. 2008;33:526–32. https://doi.org/10.1007/s11064-007-9469-8.
17. Holtzman DM, Morris JC, Goate AM. Alzheimer's disease: the challenge of the second centrury. Sci Transl Med. 2011;3:77.
18. Lin MT, Beal MF. Mitochondrial dysfunction and oxidative stress in neurodegenerative diseases. Nature. 2006;443:787–95.
19. Butterfield DA, Halliwell B. Oxidative stress, dysfunctional glucose metabolism and Alzheimer disease. Nat Rev Neurosci. 2019;20:148–60. https://doi.org/10.1038/s41583-019-0132-6.
20. Wallace DC. A mitochondrial paradigm of metabolic and degenerative diseases, aging, and cancer: a dawn for evolutionary medicine. Annu Rev Genet. 2005;39:359–407. https://doi.org/10.1146/annurev.genet.39.110304.095751.
21. Mosconi L, Berti V, Quinn C, McHugh P, Petrongolo G, Osorio RS, et al. Perimenopause and emergence of an Alzheimer's bioenergetic phenotype in brain and periphery. PLOS ONE. 2017;12:e0185926. https://doi.org/10.1371/journal.pone.0185926.
22. Mosconi L, de Leon M, Murray J, Lezi E, Lu J, Javier E, et al. Reduced mitochondria cytochrome oxidase activity in adult children of mothers with Alzheimer's disease. J Alzheimers Dis. 2011;27:483–90. https://doi.org/10.3233/JAD-2011-110866.
23. Picard M, McManus MJ. Mitochondrial signaling and neurodegeneration. In: Reeve AK, Simcox EM, Duchen MR, Turnbull DM, editors. Mitochondrial dysfunction in neurodegenerative disorders. Cham: Springer International Publishing; 2016. p. 107–37.
24. Lijia Z, Zhao S, Wang X, Wu C, Yang J. A self-propelling cycle mediated by reactive oxide species and nitric oxide exists in LPS-activated microglia. Neurochem Int. 2012;61:1220–30. https://doi.org/10.1016/j.neuint.2012.09.002.
25. Simpson DSA, Oliver PL. ROS generation in microglia: understanding oxidative stress and inflammation in neurodegenerative disease. Antioxidants Basel. 2020;9:743. https://doi.org/10.3390/antiox9080743.
26. West AP, Khoury-Hanold W, Staron M, Tal MC, Pineda CM, Lang SM, et al. Mitochondrial DNA stress primes the antiviral innate immune response. Nature. 2015;520:553–7. https://doi.org/10.1038/nature14156.
27. Nakahira K, Haspel JA, Rathinam VA, Lee SJ, Dolinay T, Lam HC, et al. Autophagy proteins regulate innate immune responses by inhibiting the release of mitochondrial DNA mediated by the NALP3 inflammasome. Nat Immunol. 2011;12:222–30. https://doi.org/10.1038/ni.1980.
28. Park J, Min JS, Kim B, Chae UB, Yun JW, Choi MS, et al. Mitochondrial ROS govern the LPS-induced pro-inflammatory response in microglia cells by regulating MAPK and NF-kappaB pathways. Neurosci Lett. 2015;584:191–6. https://doi.org/10.1016/j.neulet.2014.10.016.
29. Martinez FO, Gordon S. The M1 and M2 paradigm of macrophage activation: time for reassessment. F1000prime Reports. 2014;6:13. https://doi.org/10.12703/p6-13.
30. Qin L, Liu Y, Cooper C, Liu B, Wilson B, Hong J-S. Microglia enhance β-amyloid peptide-induced toxicity in cortical and mesencephalic neurons by producing reactive oxygen species. J Neurochem. 2002;83:973–83. https://doi.org/10.1046/j.1471-4159.2002.01210.x.
31. Shimada K, Crother TR, Karlin J, Dagvadorj J, Chiba N, Chen S, et al. Oxidized mitochondrial DNA activates the NLRP3 inflammasome during apoptosis. Immunity. 2012;36:401–14. https://doi.org/10.1016/j.immuni.2012.01.009.
32. Bianca VD, Dusi S, Bianchini E, Dal Prà I, Rossi F. Beta-amyloid activates the O-2 forming NADPH oxidase in microglia, monocytes, and neutrophils: a possible inflammatory mechanism of neuronal damage in Alzheimer's disease. J Biol Chem. 1999;274:15493–9. https://doi.org/10.1074/jbc.274.22.15493.
33. Chu W, Chepetan A, Zhou D, Shoghi KI, Xu J, Dugan LL, et al. Development of a PET radiotracer for non-invasive imaging of the reactive oxygen species, superoxide, in vivo. Org Biomol Chem. 2014;12:4421–31. https://doi.org/10.1039/c3ob42379d.
34. Hou C, Hsieh CJ, Li S, Lee H, Graham TJ, Xu K, et al. Development of a positron emission tomography radiotracer for imaging elevated levels of superoxide in neuroinflammation. ACS Chem Neurosci. 2017. https://doi.org/10.1021/acschemneuro.7b00385.
35. Cuddihy SL, Ali SS, Musiek ES, Lucero J, Kopp SJ, Morrow JD, et al. Prolonged alpha-tocopherol deficiency decreases oxidative stress and unmasks alpha-tocopherol-dependent regulation of mitochondrial function in the brain. J Biol Chem. 2008;283:6915–24. https://doi.org/10.1074/jbc.M702572200.
36. Jack CR Jr, Bennett DA, Blennow K, Carrillo MC, Dunn B, Haeberlein SB, et al. NIA-AA research framework: toward a biological definition of Alzheimer's disease. Alzheimers Dement. 2018;14:535–62. https://doi.org/10.1016/j.jalz.2018.02.018.
37. Sperling RA, Aisen PS, Beckett LA, Bennett DA, Craft S, Fagan AM, et al. Toward defining the preclinical stages of Alzheimer's disease: recommendations from the National Institute on Aging-Alzheimer's Association workgroups on diagnostic guidelines for Alzheimer's disease. Alzheimers Dement. 2011;7:280–92. https://doi.org/10.1016/j.jalz.2011.03.003.
38. Gallagher JJ, Minogue AM, Lynch MA. Impaired performance of female APP/PS1 mice in the Morris water maze is coupled with increased Aβ accumulation and microglial activation. Neurodegener Dis. 2013;11:33–41. https://doi.org/10.1159/000337458.
39. Wang J, Tanila H, Puoliväli J, Kadish I, van Groen T. Gender differences in the amount and deposition of amyloidbeta in APPswe and PS1 double transgenic mice. Neurobiol Dis. 2003;14:318–27. https://doi.org/10.1016/j.nbd.2003.08.009.
40. Guillot-Sestier MV, Araiz AR, Mela V, Gaban AS, O'Neill E, Joshi L, et al. Microglial metabolism is a pivotal factor in sexual dimorphism in Alzheimer's disease. Commun Biol. 2021;4:711. https://doi.org/10.1038/s42003-021-02259-y.
41. Ali T, Kim T, Rehman SU, Khan MS, Amin FU, Khan M, et al. Natural dietary supplementation of anthocyanins via PI3K/Akt/Nrf2/HO-1 pathways mitigate oxidative stress, neurodegeneration, and memory impairment in a mouse model of Alzheimer's disease. Mol Neurobiol. 2018;55:6076–93. https://doi.org/10.1007/s12035-017-0798-6.
42. Xie H, Hou S, Jiang J, Sekutowicz M, Kelly J, Bacskai BJ. Rapid cell death is preceded by amyloid plaque-mediated oxidative stress. Proc Natl Acad Sci. 2013;110:7904–9. https://doi.org/10.1073/pnas.1217938110.
43. Takkinen JS, López-Picón FR, Al Majidi R, Eskola O, Krzyczmonik A, Keller T, et al. Brain energy metabolism and neuroinflammation in ageing APP/PS1-21 mice using longitudinal 18F-FDG and 18F-DPA-714 PET imaging. J Cereb Blood Flow Metab. 2017;37:2870–82.
44. Lyoo CH, Ikawa M, Liow JS, Zoghbi SS, Morse CL, Pike VW, et al. Cerebellum can serve as a pseudo-reference region in Alzheimer disease to detect neuroinflammation measured with PET radioligand binding to translocator protein. J Nucl Med. 2015;56:701–6. https://doi.org/10.2967/jnumed.114.146027.
45. Guglielmotto M, Giliberto L, Tamagno E, Tabaton M. Oxidative stress mediates the pathogenic effect of different Alzheimer's disease risk factors. Front Aging Neurosci. 2010. https://doi.org/10.3389/neuro.24.003.2010.
46. de Dios C, Bartolessis I, Roca-Agujetas V, Barbero-Camps E, Mari M, Morales A, et al. Oxidative inactivation of amyloid beta-degrading

proteases by cholesterol-enhanced mitochondrial stress. Redox Biol. 2019;26:101283. https://doi.org/10.1016/j.redox.2019.101283.
47. Vainchtein ID, Molofsky AV. Astrocytes and microglia: in sickness and in health. Trends Neurosci. 2020;43:144–54. https://doi.org/10.1016/j.tins.2020.01.003.
48. Zhang L, Fang Y, Zhao X, Zheng Y, Ma Y, Li S, et al. miR-204 silencing reduces mitochondrial autophagy and ROS production in a murine AD model via the TRPML1-activated STAT3 pathway. Mol Ther Nucleic Acids. 2021;24:822–31. https://doi.org/10.1016/j.omtn.2021.02.010.
49. Smith MA, Richey Harris PL, Sayre LM, Beckman JS, Perry G. Widespread peroxynitrite-mediated damage in Alzheimer's disease. J Neurosci. 1997;17:2653–7. https://doi.org/10.1523/jneurosci.17-08-02653.1997.
50. Xie Z, Wei M, Morgan TE, Fabrizio P, Han D, Finch CE, et al. Peroxynitrite mediates neurotoxicity of amyloid beta-peptide1-42- and lipopolysaccharide-activated microglia. J Neurosci. 2002;22:3484–92. https://doi.org/10.1523/jneurosci.22-09-03484.2002.
51. Wirth M, Madison CM, Rabinovici GD, Oh H, Landau SM, Jagust WJ. Alzheimer's disease neurodegenerative biomarkers are associated with decreased cognitive function but not β-amyloid in cognitively normal older individuals. J Neurosci. 2013;33:5553–63. https://doi.org/10.1523/jneurosci.4409-12.2013.
52. McDonald DR, Brunden KR, Landreth GE. Amyloid fibrils activate tyrosine kinase-dependent signaling and superoxide production in microglia. J Neurosci. 1997;17:2284–94. https://doi.org/10.1523/jneurosci.17-07-02284.1997.
53. Meda L, Bonaiuto C, Baron P, Otvos L Jr, Rossi F, Cassatella MA. Priming of monocyte respiratory burst by beta-amyloid fragment (25–35). Neurosci Lett. 1996;219:91–4. https://doi.org/10.1016/s0304-3940(96)13177-3.
54. Keil U, Bonert A, Marques CA, Scherping I, Weyermann J, Strosznajder JB, et al. Amyloid beta-induced changes in nitric oxide production and mitochondrial activity lead to apoptosis. J Biol Chem. 2004;279:50310–20.
55. Ii M, Sunamoto M, Ohnishi K, Ichimori Y. Beta-Amyloid protein-dependent nitric oxide production from microglial cells and neurotoxicity. Brain Res. 1996;720:93–100. https://doi.org/10.1016/0006-8993(96)00156-4.
56. Ferrer-Sueta G, Radi R. Chemical biology of peroxynitrite: kinetics, diffusion, and radicals. ACS Chem Biol. 2009;4:161–77. https://doi.org/10.1021/cb800279q.
57. Malinski T. Nitric oxide and nitroxidative stress in Alzheimer's disease. J Alzheimer's Dis. 2007;11:207–18. https://doi.org/10.3233/jad-2007-11208.
58. Beckman JS, Koppenol WH. Nitric oxide, superoxide, and peroxynitrite: the good, the bad, and ugly. Am J Physiol. 1996;271:C1424–37. https://doi.org/10.1152/ajpcell.1996.271.5.C1424.
59. Mishra A, Wang Y, Yin F, Vitali F, Rodgers KE, Soto M, et al. A tale of two systems: lessons learned from female mid-life aging with implications for Alzheimer's prevention and treatment. Ageing Res Rev. 2021;74:101542. https://doi.org/10.1016/j.arr.2021.101542.
60. Finch CE, Felicio LS, Mobbs CV, Nelson JF. Ovarian and steroidal influences on neuroendocrine aging processes in female rodents. Endocr Rev. 1984;5:467–97. https://doi.org/10.1210/edrv-5-4-467.
61. Nelson JF, Felicio LS, Randall PK, Sims C, Finch CE. A longitudinal study of estrous cyclicity in aging C57BL/6J mice: I. Cycle frequency, length and vaginal cytology. Biol Reprod. 1982;27:327–39. https://doi.org/10.1095/biolreprod27.2.327.
62. Ding F, Yao J, Rettberg JR, Chen S, Brinton RD. Early decline in glucose transport and metabolism precedes shift to ketogenic system in female aging and Alzheimer's mouse brain: implication for bioenergetic intervention. PLOS ONE. 2013;8:e79977. https://doi.org/10.1371/journal.pone.0079977.
63. Brinton RD, Yao J, Yin F, Mack WJ, Cadenas E. Perimenopause as a neurological transition state. Nat Rev Endocrinol. 2015;11:393–405. https://doi.org/10.1038/nrendo.2015.82.
64. Razmara A, Duckles SP, Krause DN, Procaccio V. Estrogen suppresses brain mitochondrial oxidative stress in female and male rats. Brain Res. 2007;1176:71–81.
65. Mobbs CV, Moreno CL, Poplawski M. Metabolic mystery: aging, obesity, diabetes, and the ventromedial hypothalamus. Trends Endocrinol Metab. 2013;24:488–94.
66. Jiang CH, Tsien JZ, Schultz PG, Hu Y. The effects of aging on gene expression in the hypothalamus and cortex of mice. Proc Natl Acad Sci. 2001;98:1930–4.
67. Nilsen J, Irwin RW, Gallaher TK, Brinton RD. Estradiol in vivo regulation of brain mitochondrial proteome. J Neurosci. 2007;27:14069–77. https://doi.org/10.1523/jneurosci.4391-07.2007.
68. Rettberg JR, Yao J, Brinton RD. Estrogen: a master regulator of bioenergetic systems in the brain and body. Front Neuroendocrinol. 2014;35:8–30. https://doi.org/10.1016/j.yfrne.2013.08.001.
69. Borrás C, Gambini J, López-Grueso R, Pallardó FV, Viña J. Direct antioxidant and protective effect of estradiol on isolated mitochondria. Biochim Biophys Acta. 2010;1802:205–11. https://doi.org/10.1016/j.bbadis.2009.09.007.
70. Thakkar R, Wang R, Wang J, Vadlamudi RK, Brann DW. 17β-Estradiol regulates microglia activation and polarization in the hippocampus following global cerebral ischemia. Oxid Med Cell Longev. 2018;2018:4248526. https://doi.org/10.1155/2018/4248526.
71. Hou C, Peng Y, Qin C, Fan F, Liu J, Long J. Hydrogen-rich water improves cognitive impairment gender-dependently in APP/PS1 mice without affecting Aβ clearance. Free Radic Res. 2018;52:1311–22. https://doi.org/10.1080/10715762.2018.1460749.
72. Nair S, Sobotka KS, Joshi P, Gressens P, Fleiss B, Thornton C, et al. Lipopolysaccharide-induced alteration of mitochondrial morphology induces a metabolic shift in microglia modulating the inflammatory response in vitro and in vivo. Glia. 2019;67:1047–61. https://doi.org/10.1002/glia.23587.
73. Mirrione MM, Schiffer WK, Fowler JS, Alexoff DL, Dewey SL, Tsirka SE. A novel approach for imaging brain–behavior relationships in mice reveals unexpected metabolic patterns during seizures in the absence of tissue plasminogen activator. Neuroimage. 2007;38:34–42.
74. Sawiak S, Wood N, Williams G, Morton A, Carpenter T. SPMMouse: a new toolbox for SPM in the animal brain. In: ISMRM 17th scientific meeting and exhibition, April; 2009. p. 18–24.

Publisher's Note

Springer Nature remains neutral with regard to jurisdictional claims in published maps and institutional affiliations.

Submit your manuscript to a SpringerOpen journal and benefit from:

- ► Convenient online submission
- ► Rigorous peer review
- ► Open access: articles freely available online
- ► High visibility within the field
- ► Retaining the copyright to your article

Submit your next manuscript at ► springeropen.com